

## Article

# Effect of SiC Particle Contents and Size on the Microstructure and Dissolution of SiC-Hydroxyapatite Coatings

Li Yang <sup>1,\*</sup> and Zuli Mao <sup>2,3</sup><sup>1</sup> School of Chemical and Environmental Engineering, Hunan Institute of Technology, Hengyang 421000, China<sup>2</sup> Research Institute of Automobile Parts Technology, Hunan Institute of Technology, Hengyang 421000, China; maomao5657@yeah.net<sup>3</sup> National Joint Engineering Laboratory of Automobile Pump Parts Design and Manufacturing, Hengyang 421000, China

\* Correspondence: yangch\_1234@sina.com

**Abstract:** Carbon/carbon composites, when used as bone implant materials, do not adhere well to the bone tissues because of their non-bioactive characteristics. Therefore, we electro-deposited SiC-hydroxyapatite coatings (with an ultrasound-assisted step) on carbon/carbon composites. We analyzed how the content and size of the SiC particles affected the structure, morphology, bonding strength and dissolution of the SiC-hydroxyapatite coatings. The hydroxyapatite coating dissolution properties were assessed by the released Ca<sup>2+</sup> and the weight loss. The SiC-hydroxyapatite coating on naked carbon/carbon composites showed a more compact microstructure in comparison to the hydroxyapatite coating on carbon/carbon composites. The reasons for the changes in the microstructure and the improvement in the adhesion of the coatings on C/C were discussed. Moreover, the addition of SiC particles increased the binding strengths of the hydroxyapatite coating on C/C composite, as well as reduced the dissolution rate of the hydroxyapatite coating.



**Citation:** Yang, L.; Mao, Z. Effect of SiC Particle Contents and Size on the Microstructure and Dissolution of SiC-Hydroxyapatite Coatings.

*Coatings* **2021**, *11*, 1166. <https://doi.org/10.3390/coatings11101166>

Academic Editor: Anatoly Kovalev

Received: 18 August 2021

Accepted: 23 September 2021

Published: 27 September 2021

**Publisher's Note:** MDPI stays neutral with regard to jurisdictional claims in published maps and institutional affiliations.



**Copyright:** © 2021 by the authors. Licensee MDPI, Basel, Switzerland. This article is an open access article distributed under the terms and conditions of the Creative Commons Attribution (CC BY) license (<https://creativecommons.org/licenses/by/4.0/>).

**Keywords:** carbon/carbon composites; hydroxyapatite-SiC coatings; microstructure; binding strengths; dissolution

## 1. Introduction

The ease of designability, excellent biocompatibility and mechanical properties similar to natural bones make carbon/carbon (C/C) composites excellent bone implant materials [1,2]. However, C/C composites do not bond strongly to the bone tissues because they are non-bioactive [3]. Thus, a technology for enhancing the C/C composite bioactivity is needed. One way to achieve this is to coat C/C composites with bioactive coatings [4,5].

Hydroxyapatite (HA) possesses an excellent bioactivity and is often applied as a coating to promote the osseointegration of implant materials [6–8]. Wen et al. [9] hydrothermally synthesized a hydroxyapatite coating on a medical magnesium alloy surface and analyzed its corrosion resistance. Lo et al. [10] developed a straightforward hydrothermal synthesis and used a mixture of calcium hydroxide and sodium tripolyphosphate to obtain a structurally tunable hydroxyapatite coating on a Ti-6Al-4V surface. A hydroxyapatite coating was also applied to C/C composites and significantly improved their bioactivity [11,12]. For example, Xiong et al. [13] prepared adhesive hydroxyapatite coatings on C/C composites to improve their bioactivity-related properties. Liu et al. [14] synthesized a SiO<sub>2</sub>-reinforced hydroxyapatite coating on similar C/C composites by a combination of hydrothermal electrochemical deposition and hydrothermal treatment. However, hydroxyapatite coatings are brittle, which often worsens the mechanical properties of the corresponding implants. Additionally, hydroxyapatite does not bind well to C/C composites [15,16]. To solve this problem and to reinforce the hydroxyapatite coating, Li et al. [17] added TiO<sub>2</sub> and observed an improved Young's modulus, fracture toughness and shear strength of the resulting TiO<sub>2</sub>-HA composite coatings prepared using high-velocity oxyfuel

spraying. Mihailescu et al. [18] reinforced HA by  $MgF_2$  and  $MgO$  particles and obtained a material with an excellent adherence and biological performance. Liu et al. [19] improved the HA coating bonding strength to C/C composites by applying a tree-planting interface structure. Fu et al. [20] improved the cohesion strength of a hydroxyapatite (HA) coating on C/C composites by adding SiC nanowires.

The excellent biocompatibility, wear resistance and stability of SiC make it a promising material for biological applications [21–25]. Particularly, the chemical inertness makes SiC useful as a material for the bearing surface of implants [3,26]. The incorporation of small amounts of SiC particles around the implants was proven to be a safe approach, capable of stimulating the growth of bone tissues [27–30]. SiC-containing coatings were also used on stents to enhance their hemocompatibility and bonding strength [30]. Vladescu et al. [31] coated HA coatings with a SiC layer and obtained a material with excellent hardness and other mechanical properties. Fu et al. [3] reported SiC nanowires which formed pinning at the HA coating/matrix interface, which in turn enhanced the bonding strength at the interface and provided a three-dimensional framework. This improved the overall HA coating cohesion.

This work demonstrated an approach to obtain an improved bonding strength between the hydroxyapatite coating and the substrate, which was achieved by incorporating SiC particles using ultrasonic-assisted electrodeposition. This paper discusses how the SiC particle sizes and contents in the coating affect the bonding strength and solubility of the HA-based composite material.

## 2. Materials and Methods

Several pieces ( $10\text{ mm} \times 10\text{ mm} \times 1.5\text{ mm}$ ) were cut from a large C/C composite sheet (obtained using chemical vapor deposition) with a  $1.2\text{--}1.3\text{ g/cm}^3$  density, polished using 600 grit SiC paper, cleaned with distilled water, dried at  $100\text{ }^\circ\text{C}$  for 2 h, and then soaked in  $H_2O_2$  for 24 h, followed by distilled water rinsing and drying at  $150\text{ }^\circ\text{C}$  for 2 h.

To prepare HA coatings, we used  $Ca(NO_3)_2$  and  $3\text{ mmol/L NH}_4H_2PO_4$  solutions in amounts taken to maintain the Ca/P mole ratio, equal to 1.67. To prepare SiC-containing hydroxyapatite, we used commercially purchased SiC (analytically pure), which was ultrasonically cleaned with ethanol for 30 min and dried at  $70\text{ }^\circ\text{C}$  for 24 h. SiC samples with 50, 100, and 200 nm particles were used. The contents of SiC added to hydroxyapatite synthesis were equal to 0.01, 0.1 and 1 g/L.

SiC-hydroxyapatite coatings were deposited onto the substrates electrochemically at  $60\text{ }^\circ\text{C}$  for 1 h under 7 V. The resulting samples were rinsed with distilled water, dried at  $150\text{ }^\circ\text{C}$  and then treated with  $0.01\text{ mol/L NaOH}$  solution for 2 h, followed by rinsing and drying. All preparation steps are shown in Figure 1.

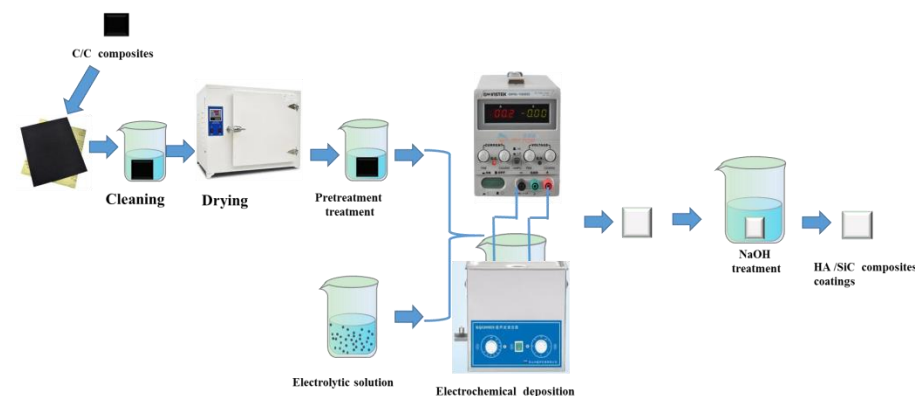


Figure 1. Experimental flow graph.

The sample crystallinity, morphology, and composition were obtained using X-ray diffraction (XRD, performed using Bruker D8ADVANCE instrument, Billerica, Massachusetts, USA) and scanning electron microscopy (SEM, performed using Hitachi S-4800, Tokyo, Japan;

Zeiss Sigma 300 setups, Jena, Germany) coupled with the energy dispersive spectroscopy. For SEM, all samples were coated with a thin layer of Au. Fourier transform infrared (FTIR, performed using IRAffinity-1s, shimadzu corporation, Kyoto, Japan) spectroscopy performed using a Shimadzu instrument was used to identify the surface functionality of the coatings.

The binding strength was tested with a scratch tester. The micron grade scratch tests were tested on micron grade scratch tester (MCT, Swiss CSM Instrument Co., Ltd., Peseux, Switzerland). For this purpose, four samples were prepared for each combination of SiC contents/particle size. The final value was reported as an average of four measurements.

The dissolution rates of the SiC-hydroxyapatite coating samples were measured using physiological saline solution (0.9% NaCl) at 36.5 °C. For this purpose, the hydroxyapatite coating pieces with a known weight were soaked for 1, 3, 5, 7, and 14 days, followed by a measuring of their Ca ion concentration and weight loss examination. For each coating composition and duration, four parallel tests were performed. After sampling 5 mL of the mother solution after 14 days of immersion, an appropriate amount of dilute nitric acid solution was added to the remaining solution. Additionally, 5 mL was of the mother solution was taken out again after the precipitates were completely dissolved. The resulting sample was named "14R". After the dissolution tests, the Ca<sup>2+</sup> content in the saline solution was detected by the inductively coupled plasma-mass spectrometry (ICP-MS, Thermo Tisher Scientific, Waltham, MA, USA).

### 3. Results

#### 3.1. Effect of SiC Particle Sizes on the Hydroxyapatite Coating Properties

To analyze the effect of the SiC particles on the properties of the resulting hydroxyapatite coatings, we added 1 g/L SiC particles with average sizes equal to 50, 100, and 200 nm during the hydroxyapatite coating preparation. The XRD of the resulting samples showed the presence of the peaks attributed to the carbon matrix, hydroxyapatite coating and SiC particles (see Figure 2). The XRD peak intensity for the SiC phase gradually increased as the SiC particle size increased and was strongest for the hydroxyapatite coating containing 200 nm SiC particles. Additionally, as the SiC particle size increased, the intensity of the hydroxyapatite peaks increased and was the highest for the hydroxyapatite coating containing 200 nm SiC particles. No other peaks were observed in the XRD spectra of our SiC-hydroxyapatite samples. Thus, SiC and hydroxyapatite did not react strongly enough to form additional phases (see Figure 2).

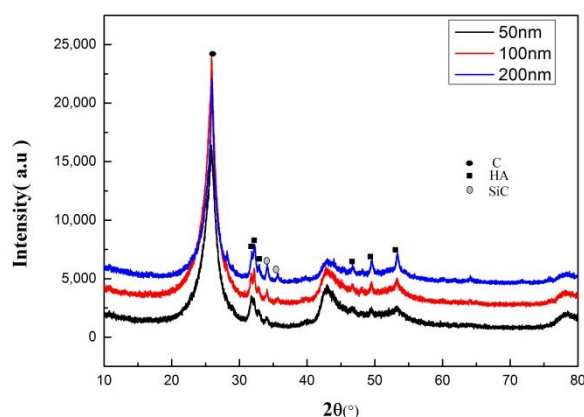


**Figure 2.** X-ray diffraction of SiC-hydroxyapatite coatings under different SiC particle sizes.

The SEM of the SiC-hydroxyapatite coatings revealed some flaws (see Figure 3a). The SiC-hydroxyapatite coating containing 50 nm SiC particles contained short rod-like features and particles with numerous small holes (see Figure 3b). The coatings which contained larger SiC particles possessed a more fibrous morphology. The SiC-hydroxyapatite coatings containing 200 nm SiC particles possessed an interwoven fibrous morphology (see Figure 3d) with some lumpy tissues above the fibers.

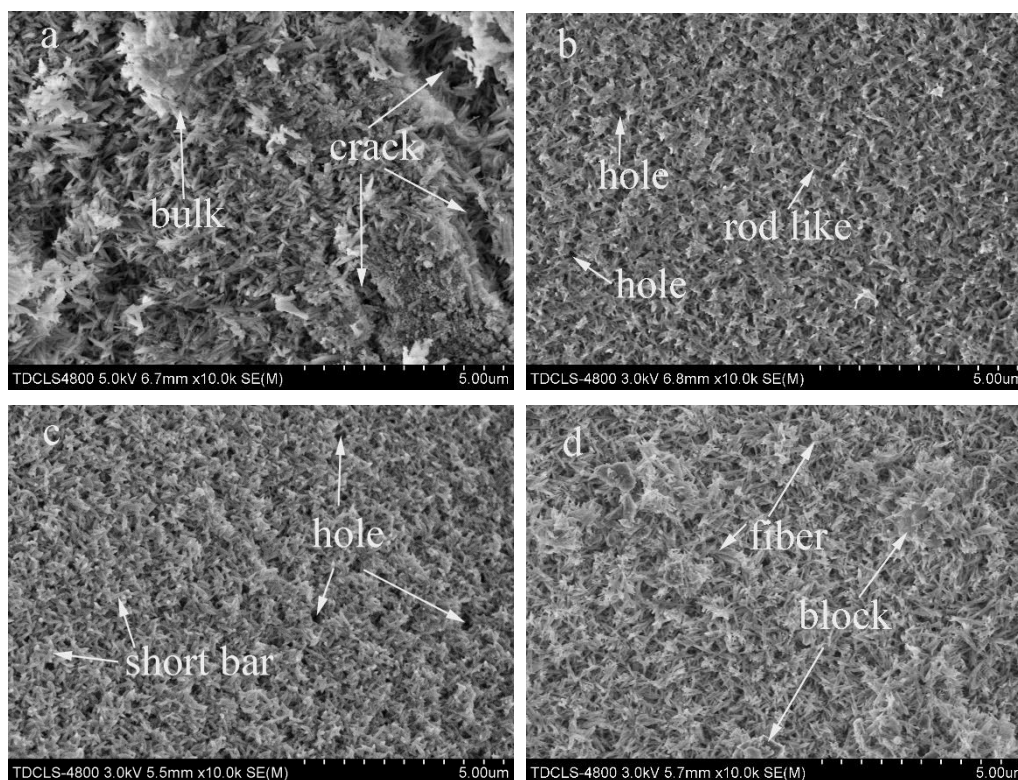


**Figure 3.** Surface morphology and EDS of SiC-hydroxyapatite coatings with different SiC particle sizes: (a) hydroxyapatite; (b) hydroxyapatite + 50 nm SiC; (c) hydroxyapatite + 100 nm SiC; (d) hydroxyapatite + 200 nm SiC.

The FTIR spectra of the SiC-hydroxyapatite coatings showed peaks at  $948$  and  $1032\text{ cm}^{-1}$  (see Figure 4), which belonged to  $\text{PO}_4^{3-}$  vibrations [31]. Additional bands at  $556$  and  $605\text{ cm}^{-1}$  were attributed to the  $m_4$  vibrational mode of the P-O bond in the  $\text{PO}_4^{3-}$  groups [32]. The band at  $940\text{--}960\text{ cm}^{-1}$  was ascribed to the Si-C stretching bond [33]. The peaks in the  $1460\text{--}1530\text{ cm}^{-1}$  range corresponded to the  $\text{CO}_3^{2-}$  formed due to the atmospheric  $\text{CO}_2$  dissolution in the solutions during the sample preparation [34]. The bands at  $1570\text{--}1640\text{ cm}^{-1}$  and  $3440\text{--}3450\text{ cm}^{-1}$  were ascribed to the absorbed water [35,36] while the peak at  $3570\text{ cm}^{-1}$  was ascribed to the OH vibrations.

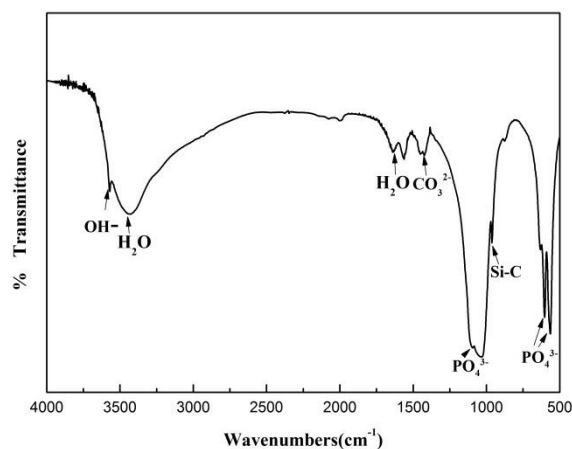


**Figure 4.** The FTIR spectra of the SiC-hydroxyapatite (200 nm, 1 g/L) coatings.

The bonding strengths between the SiC-hydroxyapatite coatings and the C/C composite's matrix were determined by scratch tests. The analysis of the chemical bonding strengths between the coatings and the C/C composites matrix showed that the bonding

strength of the hydroxyapatite coatings significantly increased when SiC was incorporated. Additionally, the overall bonding strength increased as the SiC particle increased (see Figure 5). Thus, SiC-hydroxyapatite coatings containing 200 nm SiC particles exhibited the strongest bond between the hydroxyapatite coatings and the matrix. The bonding strengths for the SiC-hydroxyapatite coatings containing 50 and 100 nm SiC particles were almost the same. The pristine hydroxyapatite coating was loose and cracked (see Figure 3a) which explained its poor mechanical and binding strength. However, the SiC-hydroxyapatite coatings containing 200 nm SiC particles were uniform and dense (see Figure 3d), which explained why their binding strength was the highest of all the coatings.

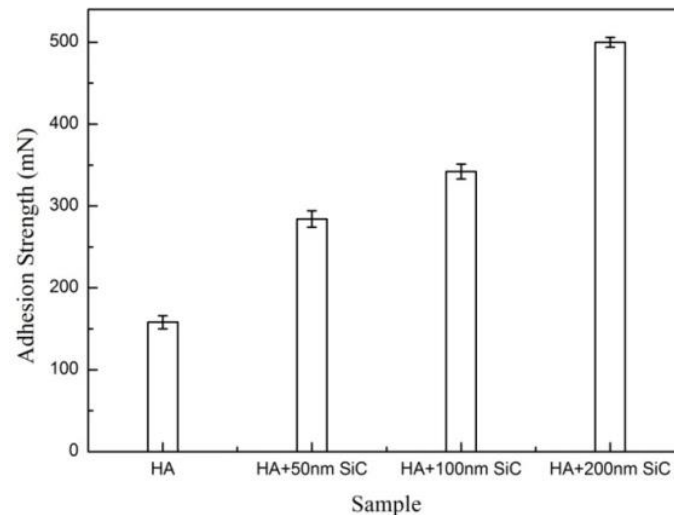


**Figure 5.** Adhesion strength of SiC-hydroxyapatite coatings at different SiC particle sizes.

### 3.2. Effect of SiC Content on HA Coating Properties

To assess how SiC contents affected the properties of the hydroxyapatite coating deposited on the C/C substrate, we added 200 nm SiC particles at the 0.01, 0.1 and 1 g/L levels. The XRD of these coatings revealed peaks belonging to the C/C composites substrate, hydroxyapatite coatings and SiC particles (see Figure 6). As the SiC content increased, the intensities of these peaks did not change, indicating that the increased SiC particle content did not affect the structure and phase formation of the SiC-hydroxyapatite coatings on the C/C composites substrate.

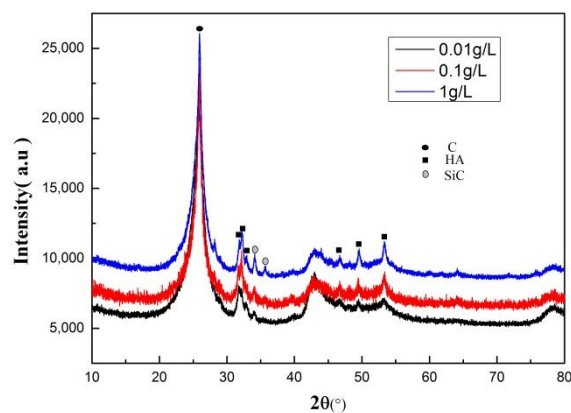


**Figure 6.** X-ray diffraction of SiC-hydroxyapatite coatings at different SiC particle (200 nm) concentrations.

The SEM of the SiC-hydroxyapatite coatings prepared using 0.01 g/L of 200 nm SiC particles showed rod-like features with small holes (see Figure 7a). The SEM of the SiC-hydroxyapatite coating prepared using 0.1 g/L of 200 nm SiC particles revealed flake-like

tissues with large voids between them (see Figure 7b). The SiC-hydroxyapatite coatings prepared using 1 g/L of 200 nm SiC exhibited interwoven fibrous features (see Figure 7c).

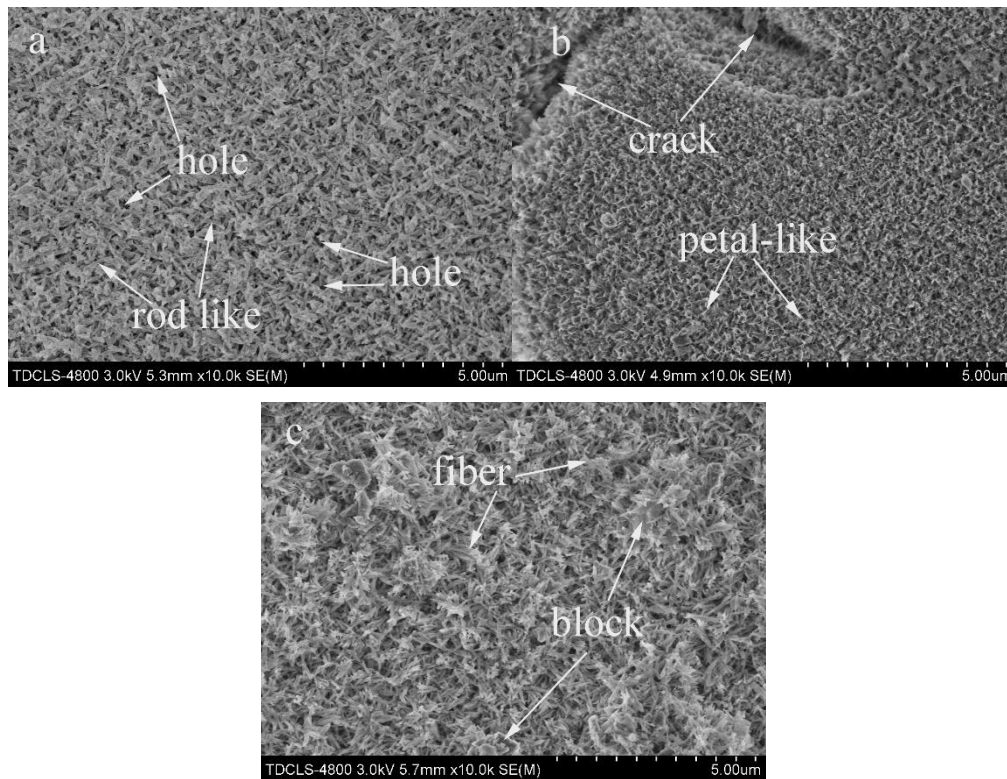


**Figure 7.** Surface morphology and EDS of SiC-hydroxyapatite coatings at different concentrations of SiC particles: (a) 0.01 g/L; (b) 0.1 g/L; (c) 1 g/L.

The cross-section sample was polished using 600 grit SiC paper and 3000 grit SiC paper, cleaned with distilled water, then dried at 100 °C for 2 h. The EDS of the cross-section of the SiC-hydroxyapatite coatings deposited on the C/C substrate showed that the coating was 20–30 µm thick (see Figure 8). The SiC-hydroxyapatite coatings were clearly observed on the surface of the C/C composite with SiC particles embedded in hydroxyapatite (see Figure 8). The binding strength diagram of the C/C composites substrate and SiC-hydroxyapatite coating showed a tight interface without cracks, with the SiC-hydroxyapatite coatings penetrating the pores of the C/C composites substrate. Thus, the binding force between the coating and the matrix could be further improved.

Figure 9 shows the binding strength between the C/C composites matrix and SiC-hydroxyapatite coatings with the 200 nm SiC particles embedded at different levels. The highest binding force was observed when 1 g/L of 200 nm SiC particles was used during the preparation of the SiC-hydroxyapatite coating. The lowest binding force was observed at the 0.1 g/L level, which confirmed the results described above (in Figure 7). The structure of the coatings could explain such a weak binding force; the microstructure of hydroxyapatite coating prepared using 0.1 g/L of 200 nm SiC particles was petal-like and demonstrated numerous large cracks. A coating with such morphology was intrinsically fragile, its cracks propagated more easily, and its active material fell off. All these factors contributed to the weak adhesion between SiC-hydroxyapatite coatings and C/C composites.

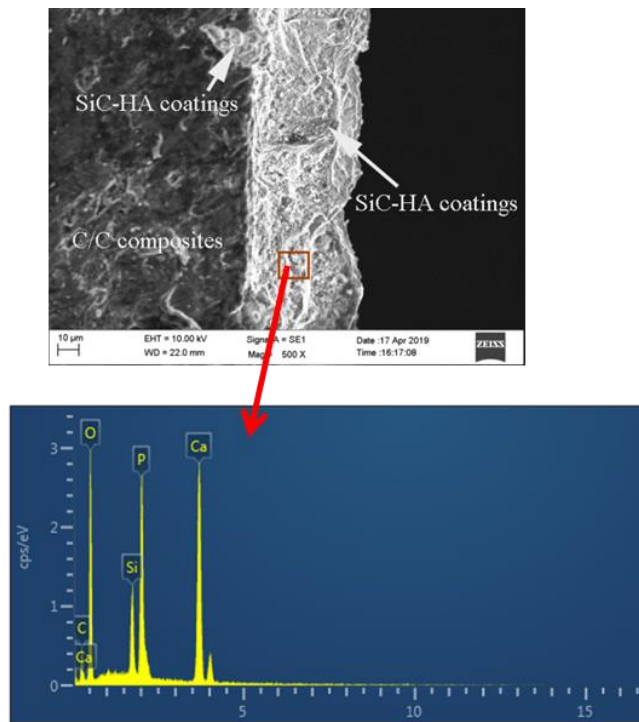


**Figure 8.** The cross section of SiC-hydroxyapatite coatings with 200 nm SiC particles.

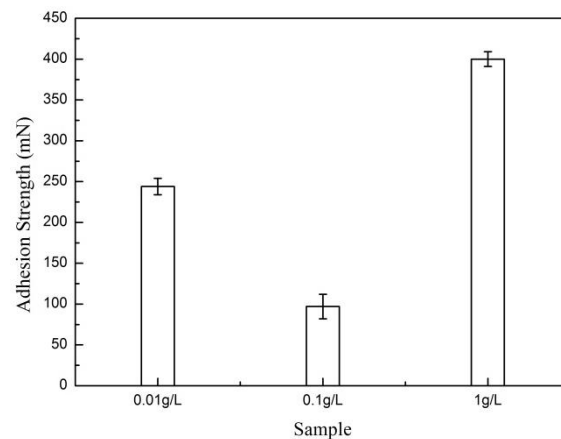


**Figure 9.** Adhesion strength of SiC-hydroxyapatite coatings at different concentrations of 200 nm SiC particles.

### 3.3. Dissolution of SiC-Hydroxyapatite Coatings

Dissolution is controlled by the processes occurring on the crystal surface, including the ion transport from the surface into the solution [37]. Figures 10 and 11 show the  $\text{Ca}^{2+}$  concentration contents in the leachate after 1–14 days of soaking SiC-hydroxyapatite coatings in physiological saline solution. As expected, the  $\text{Ca}^{2+}$  concentration in the leachate increased with the immersion time. However, all hydroxyapatite coatings, independently of their SiC particle sizes and contents, showed similar  $\text{Ca}^{2+}$  concentration contents on days 1–14 (see Figure 10).

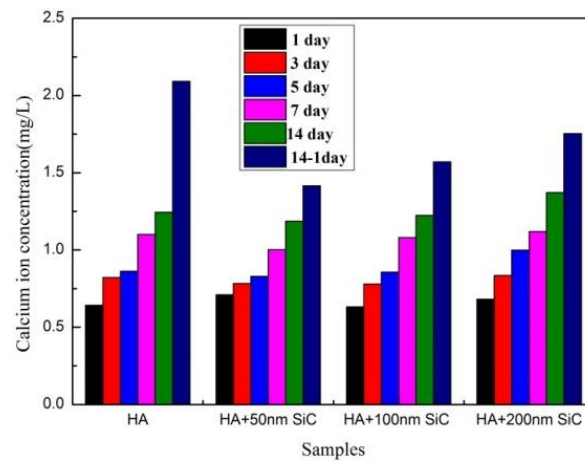


**Figure 10.** Calcium concentration of different SiC particle sizes.

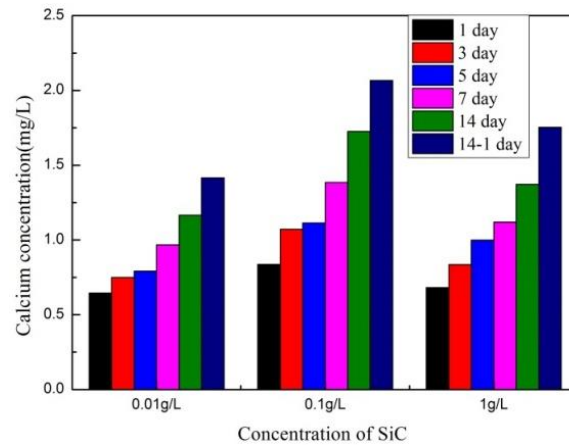


**Figure 11.** Calcium concentration of different SiC particle (200 nm) concentrations.

However, the data obtained for our coatings for the 1–14 days of soaking were significantly different. The  $\text{Ca}^{2+}$  concentration was the highest when the coating contained no SiC particles. The  $\text{Ca}^{2+}$  contents on days 14 and 14R were also very different because loosening the hydroxyapatite caused large coating pieces to detach. However, they were still too large to dissolve completely. The concentration of dissolved  $\text{Ca}^{2+}$  also did not differ significantly from day 1 to day 14 for all coatings (see Figure 11). The  $\text{Ca}^{2+}$  concentration in the leachate of the hydroxyapatite coating prepared using 0.1 g/L of 200 nm SiC particles was the highest (see Figure 11) because the corresponding SiC-hydroxyapatite coatings were loose with many cracks, which weakened their bonding strength.

The weight losses of the SiC-hydroxyapatite coatings agreed with the results discussed above on the  $\text{Ca}^{2+}$  content in the leachate (see Figures 12 and 13). The pristine hydroxyapatite coating lost the most weight (see Figure 12). The  $\text{Ca}^{2+}$  concentration content in the leaching solution was largest after 14 days of soaking in dilute  $\text{HNO}_3$ , which indicated the presence of large amounts of undisclosed chunks of hydroxyapatite coatings due to the coating peeling off during the soaking. Our data indicated that SiC presence in the hydroxyapatite inhibited its dissolution rate. The highest weight loss was observed for the SiC-hydroxyapatite coatings prepared using 0.1 g/L of 200 nm SiC particles (see Figure 13), which agreed with the data discussed above on the coating structure and morphology (see Figure 7b).

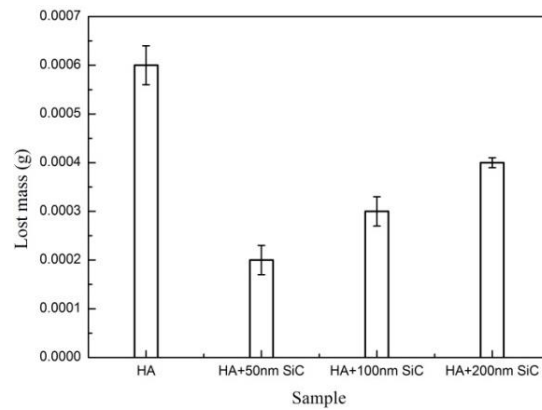


**Figure 12.** Lost mass of SiC-hydroxyapatite coatings with different SiC particle sizes.

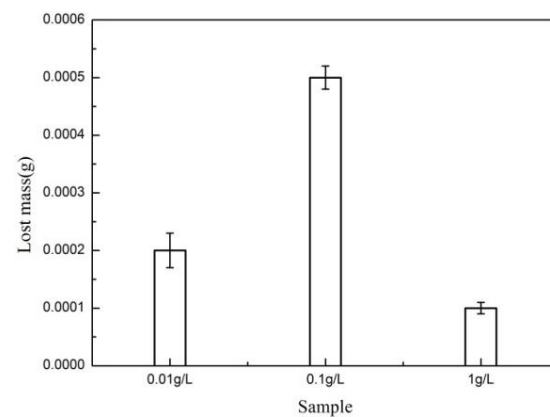


**Figure 13.** Lost mass of SiC-hydroxyapatite different SiC particle (200 nm) concentrations.

Figures 14 and 15 show the morphologies of our SiC-hydroxyapatite coatings after dissolution tests. Large pieces of hydroxyapatite coating were detached, leaving large holes (see Figure 14a) and cracks. These processes contributed to the coating weight losses and the  $\text{Ca}^{2+}$  leaching out. The prolonged dissolution tests resulted in the formation of the larger holes and shorter rods tapered at both ends (see Figure 14b) as well as honeycomb-like features (see Figure 14c). As a result, the content of the short bar-like coating features (shown in Figure 3c) decreased, which implied their dissolution and the formation of honeycombs from the less soluble coating components. The fiber-like features on the coating surface also dissolved, leaving the granular tissues (see Figure 14d), and leading to  $\text{Ca}^{2+}$  and weight losses.

Figure 15a also shows numerous holes in the coating as well as an indication that the rod-like tissue became fibrous as the coatings were soaked in the diluted  $\text{HNO}_3$ . Most of the petal-like tissues also dissolved, forming more holes (see Figure 15b). Thus, we concluded that the petal-like structures dissolved very quickly. Figure 15c also shows that the coatings' fibrous tissues dissolved, leaving granular tissues. These data confirm that the solubility of the SiC-hydroxyapatite coatings strongly depended on their microstructure and morphology, both of which, in turn, were defined by the content and size of the embedded SiC particles.

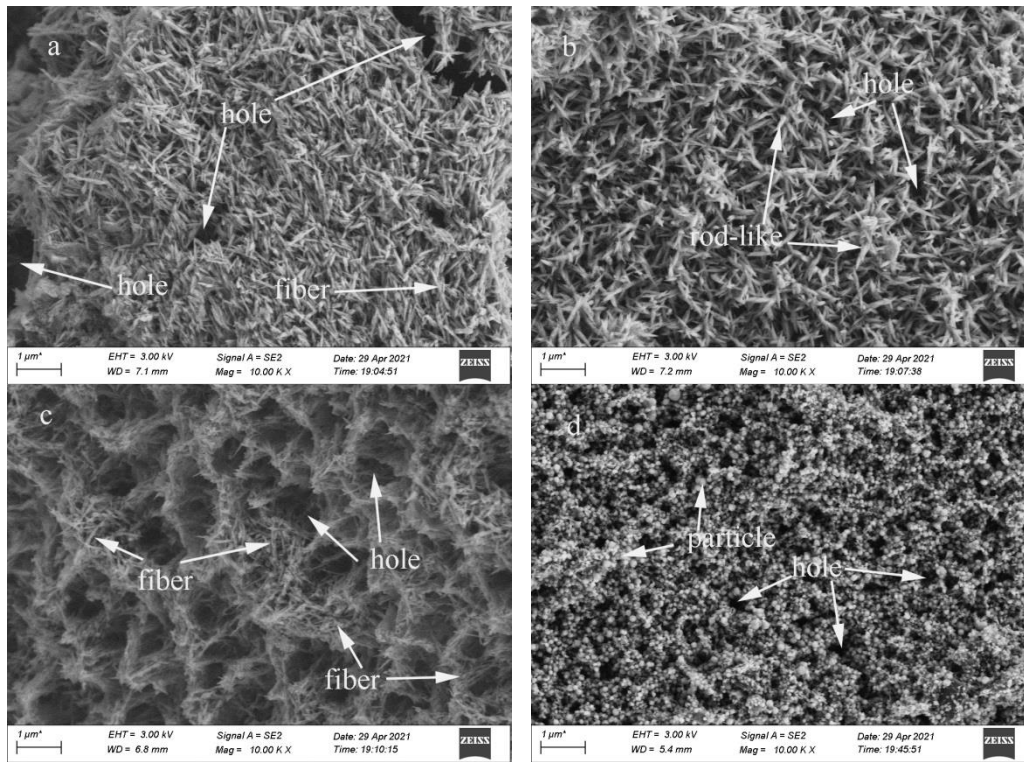


**Figure 14.** Surface morphology of SiC-hydroxyapatite coatings with different SiC particle sizes after dissolution: (a) original sample; (b) 50 nm; (c) 100 nm; (d) 200 nm.

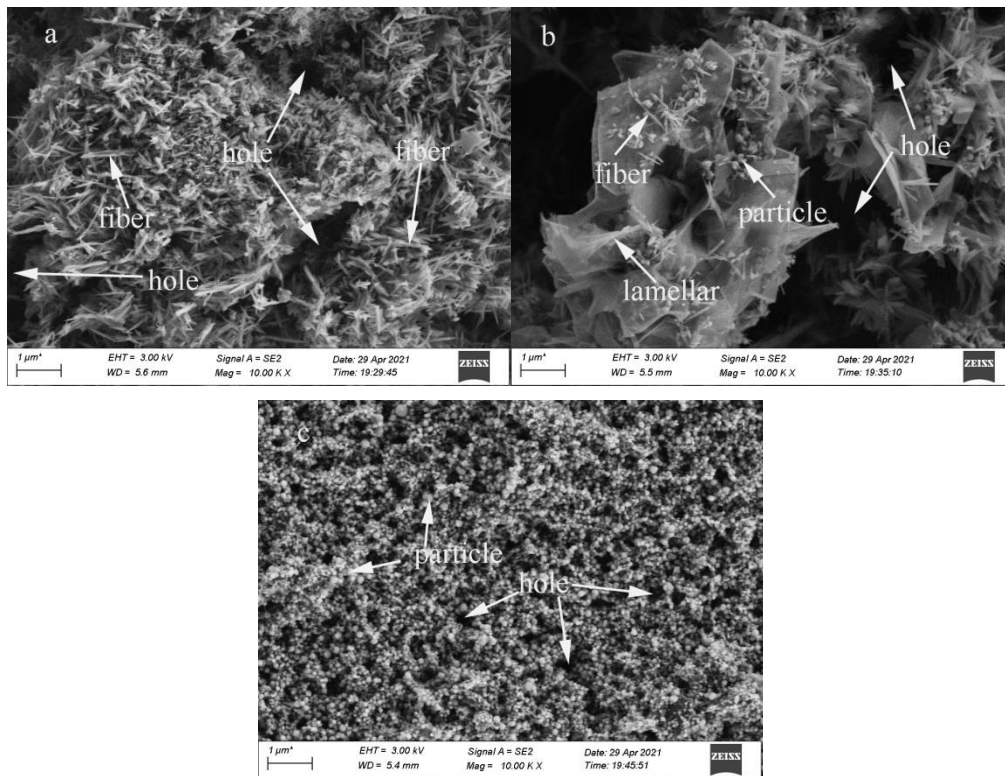


**Figure 15.** Surface morphology of SiC-hydroxyapatite coatings with different SiC particle (200 nm) concentration after dissolution: (a) 0.01 g/L; (b) 0.1 g/L; (c) 1 g/L.

#### 4. Conclusions

Nano-SiC particles were introduced into hydroxyapatite coatings to improve their binding strengths to the C/C substrates. The structures, morphologies and binding strengths of the resulting SiC-hydroxyapatite coatings were studied as functions of the SiC particle contents and sizes. As the sizes of the embedded SiC particles increased, the hydroxyapatite diffraction peaks of the corresponding SiC-hydroxyapatite coatings also increased. However, the SiC content did not affect the diffraction peak strength. The SiC particle presence improved the adhesion of the hydroxyapatite coating to the C/C substrate. The best bonding strength was obtained for the coating prepared using 1 g/L of 200 nm SiC particles. The addition of the SiC nanoparticles to the hydroxyapatite coatings changed their morphologies and microstructures, which, in turn, directly correlated with the hydroxyapatite coating dissolution.

**Author Contributions:** Conceptualization, L.Y. and Z.M.; formal analysis and data curation, Z.M.; writing—original draft preparation, L.Y. All authors have read and agreed to the published version of the manuscript.

**Funding:** This research was funded by the Hengyang Science and Technology Development Project (No.2016KG67), Hunan Provincial Department of Education(No.19C0534), Hengyang Science and Technology Department (2015KS21) and Hunan Institute of Technology(No.KFB20019).

**Institutional Review Board Statement:** Not applicable.

**Informed Consent Statement:** Not applicable.

**Data Availability Statement:** The data presented in this study are available on request from the corresponding author.

**Conflicts of Interest:** The authors declare no conflict of interest.

#### References

1. Zhang, L.L.; Li, H.J.; Li, K.Z.; Zhang, Y.L.; Liu, S.J.; Guo, Q.; Li, S.X. Micro-oxidation treatment to improve bonding strength of Sr and Na co-substituted hydroxyapatite coatings for carbon/carbon composites. *Appl. Surf. Sci.* **2016**, *378*, 136–141. [[CrossRef](#)]
2. Cao, N.; Dong, J.W.; Wang, Q.X.; Ma, Q.S.; Wang, F.; Chen, H.Y.; Xue, C.Q.; Li, M.S. Plasma sprayed hydroxyapatite coating on carbon/carbon composite scaffolds for bone tissue engineering and related tests in vivo. *J. Biomed. Mater. Res. Part A* **2010**, *3*, 1019–1027. [[CrossRef](#)]
3. Zhai, Y.Q.; Li, K.Z.; Li, H.J.; Wang, C.; Liu, H. Influence of NaF concentration on fluorine-containing hydroxyapatite coating on carbon/carbon composites. *Mater. Chem. Phys.* **2007**, *106*, 22–26. [[CrossRef](#)]
4. Zhang, L.L.; Li, S.X.; Li, H.J.; Pei, L.N. Bioactive surface modification of carbon/carbon composites with multilayer SiC-SiC nanowire-Si doped hydroxyapatite coating. *J. Alloys Compd.* **2018**, *740*, 109–117. [[CrossRef](#)]
5. Ni, X.Y.; Tang, X.B.; Lin, T.; Zhao, Q.D.; Geng, C.R.; Cai, L.M.; Gao, W.D.; Miao, Y.L.; Chen, D. Properties of plasma-spray coated hydroxyapatite on carbon/carbon composites pretreated by an argon plasma. *Carbon* **2013**, *63*, 594–595. [[CrossRef](#)]
6. Vilardella, A.M.; Cinca, N.; Garcia-Giralt, N.; Dostaa, S.; Canoa, I.G.; Nogués, X.; Guilemany, J.M. In-vitro comparison of hydroxyapatite coatings obtained by cold spray and conventional thermal spray technologies. *Mater. Sci. Eng. C* **2020**, *107*, 110306. [[CrossRef](#)] [[PubMed](#)]
7. Jiang, J.W.; Han, G.; Zheng, X.S.; Chen, G.; Zhu, P.Z. Characterization and biocompatibility study of hydroxyapatite coating on the surface of titanium alloy. *Surf. Coat. Technol.* **2019**, *375*, 645–651. [[CrossRef](#)]
8. Chambard, M.; Marsan, O.; Charvillat, C.; Grossin, D.; Fort, P.; Rey, C.; Gitzhofer, F.; Bertrand, G. Effect of the deposition route on the microstructure of plasma-sprayed hydroxyapatite coatings. *Surf. Coat. Technol.* **2019**, *371*, 68–77. [[CrossRef](#)]
9. Wen, S.F.; Liu, X.L.; Ding, J.H.; Liu, Y.L.; Lan, Z.T.; Zhang, Z.M.; Chen, G.M. Hydrothermal synthesis of hydroxyapatite coating on the surface of medical magnesium alloy and its corrosion resistance. *Prog. Nat. Sci. Mater. Int.* **2021**, *31*, 324–333. [[CrossRef](#)]
10. Lo, Y.S.; Chang, C.C.; Lin, P.-C.; Lin, S.P.; Wang, C.L. Direct growth of structurally controllable hydroxyapatite coating on Ti-6Al-4V through a rapid hydrothermal synthesis. *Appl. Surf. Sci.* **2021**, *556*, 149672. [[CrossRef](#)]
11. Cao, N.; Yang, Z.G.; Yang, B.; Wang, W.B.; Boukherroub, R.; Li, M. Construction of a bone-like surface layer on hydroxyl-modified carbon/carbon composite implants via biomimetic mineralization and in vivo tests. *RSC Adv.* **2016**, *6*, 9370–9378. [[CrossRef](#)]
12. Cao, N.; Dong, J.W.; Wang, Q.X.; Ma, Q.S.; Xue, C.Q.; Li, M.S. An experimental bone defect healing with hydroxyapatite coating plasma sprayed on carbon/carbon composite implants. *Surf. Coat. Technol.* **2010**, *205*, 1150–1156. [[CrossRef](#)]
13. Xiong, X.B.; Liu, L.; Ma, J.; Ni, X.Y.; Li, Y.Y.; Zeng, X.R. A simplified process for preparing adhesive hydroxyapatite coatings on carbon/carbon composites. *Surf. Coat. Technol.* **2019**, *377*, 124925. [[CrossRef](#)]

14. Liu, L.; Ni, X.Y.; Xiong, X.B.; Ma, J.; Zeng, X.R. Low temperature preparation of SiO<sub>2</sub> reinforced hydroxyapatite coating on carbon/carbon composites. *J. Alloys Compd.* **2019**, *788*, 768–778. [[CrossRef](#)]
15. Guan, K.J.; Zhang, L.L.; Zhu, F.Y.; Li, H.J.; Sheng, H.C.; Guo, Y. Multi-layer SiC-graphene oxide-hydroxyapatite bioactive coating for carbon/carbon composites. *J. Alloys Compd.* **2020**, *821*, 153543. [[CrossRef](#)]
16. Zhang, L.L.; Li, H.J.; Li, K.Z.; Zhang, S.Y.; Fu, Q.G.; Zhang, Y.L.; Lu, J.H.; Li, W. Preparation and characterization of carbon/SiC nanowire/Na-doped carbonated hydroxyapatite multilayer coating for carbon/carbon composites. *Appl. Surf. Sci.* **2014**, *313*, 85–92. [[CrossRef](#)]
17. Li, H.; Khor, K.A.; Cheang, P. Titanium dioxide reinforced hydroxyapatite coatings deposited by high velocity oxy-fuel (HVOF) spray. *Biomaterials* **2002**, *23*, 85–91. [[CrossRef](#)]
18. Natalia, M.; Stan, G.E.; Duta, L.; Mariana, C.C.; Coralia, B.; Sopronyi, M.; Luculescu, C.; Oktar, F.N.; Mihailescu, I.N. Structural, compositional, mechanical characterization and biological assessment of bovine-derived hydroxyapatite coatings reinforced with MgF<sub>2</sub> or MgO for implants functionalization. *Mater. Sci. Eng. C* **2016**, *59*, 863–874. [[CrossRef](#)]
19. Liu, Y.Y.; Zhang, L.L.; Guan, K.J.; Wang, Z.K.; Wang, Y.T.; Li, H.P.; Lei, X.Y.; Zhang, W.X.; Wang, K.; Hu, Y.Y. Boosting bonding strength of hydroxyapatite coating for carbon/carbon composites via applying tree-planting interface structure. *Ceram. Int.* **2021**, *47*, 11922–11928. [[CrossRef](#)]
20. Fu, Q.G.; Gu, C.G.; Li, H.J.; Chu, Y.H.; Lu, J.H.; Zhang, L.L. Microstructure and mechanical properties of SiC nanowires reinforced hydroxyapatite coating on carbon/carbon composites. *Mater. Sci. Eng. A* **2013**, *563*, 133–137. [[CrossRef](#)]
21. Zhao, F.; Zhang, L.L.; Guo, Y.; Sheng, H.C.; Zhang, P.X.; Zhang, Y.X.; Li, Q.; Yang, H.Y.; Mikhailovsky, S.V. Mechanically strong and bioactive carbon fiber-SiC nanowire-hydroxyapatite-pyrolytic carbon composites for bone implant application. *Ceram. Int.* **2021**, *47*, 3389–3400. [[CrossRef](#)]
22. Hosseini, M.R.; Ahangari, M.; Johar, M.H.; Allahkaram, S.R. Optimization of nano HA-SiC coating on AISI 316L medical grade stainless steel via electrophoretic deposition. *Mater. Lett.* **2021**, *285*, 129097. [[CrossRef](#)]
23. Tao, L.; Li, X.L.; Hu, S.X.; Wu, J. Enhanced osteoporotic effect of silicon carbide nanoparticles combine with nano-hydroxyapatite coated anodized titanium implant on healthy bone regeneration in femoral fracture. *J. Photochem. Photobiol. B Biol.* **2019**, *197*, 111515. [[CrossRef](#)]
24. Hnatkoa, M.; Hičáka, M.; Labudová, M.; Galusková, D.; Sedláčeka, J.; Lenčesa, Z.; Šajgalika, P. Bioactive silicon nitride by surface thermal treatment. *J. Eur. Ceram. Soc.* **2020**, *40*, 1848–1858. [[CrossRef](#)]
25. Dodevski, V.; Pagnacco, M.C.; Radović, I.; Rosić, M.; Janković, B.; Stojmenović, M.; Mitić, V.V. Characterization of silicon carbide ceramics obtained from porous carbon structure achieved by plant carbonization. *Mater. Chem. Phys.* **2020**, *245*, 122768. [[CrossRef](#)]
26. Xu, L.-L.; Shi, X.-L.; Qian, Q.; Bai, X.-H.; Xu, L.; Wang, Q.-L. Hydrothermal sterilization in silver nitrate solution endows plasma sprayed hydroxyapatite coating with antibacterial property. *Mater. Lett.* **2020**, *263*, 127258. [[CrossRef](#)]
27. Xu, M.; Girish, Y.R.; Rakesh, K.P.; Wu, P.; Manukumar, H.M.; Byrappa, S.M.; Udayabhanu; Byrappa, K. Recent advances and challenges in silicon carbide (SiC) ceramic nanoarchitectures and their applications. *Mater. Today Commun.* **2021**, *28*, 102533. [[CrossRef](#)]
28. Vladescua, A.; Birlıkb, I.; Braica, V.; Toparlib, M.; Celıkb, E.; AkAzem, F. Enhancement of the mechanical properties of hydroxyapatite by SiC addition. *J. Mech. Behav. Biomed. Mater.* **2014**, *40*, 362–368. [[CrossRef](#)]
29. Leila, C.-K.; Jafar, K.-A.; Amir, M.; Mohamadreza, E. The effect of hydroxyapatite nanoparticles on electrochemical and mechanical performance of TiC/N coating fabricated by plasma electrolytic saturation method. *Surf. Coat. Technol.* **2020**, *394*, 125817. [[CrossRef](#)]
30. Mohammad, U.; Colin, H.; Vincent, S. Fabrication, characterisation and corrosion of HA coated AZ31B Mg implant material: Effect of electrodeposition current density. *Surf. Coat. Technol.* **2020**, *385*, 125363. [[CrossRef](#)]
31. Li, K.-Z.; Guo, Q.; Zhang, L.-L.; Zhang, Y.-L.; Liu, S.-J.; Guo, K.-B.; Li, S.-X. Synthesis and characterization of Si-substituted hydroxyapatite bioactive coating for SiC-coated carbon/carbon composites. *Ceram. Int.* **2017**, *43*, 1410–1414. [[CrossRef](#)]
32. McEntire, B.-J.; Bala, B.-S.; Rahamanc, M.-N.; Chevalier, J.; Pezzotti, G. Ceramics and ceramic coatings in orthopaedics. *J. Eur. Ceram. Soc.* **2015**, *35*, 4327–4369. [[CrossRef](#)]
33. Zhang, L.-L.; Pei, L.-N.; Li, H.-J.; Zhu, F.-Y. Design and fabrication of pyrolytic carbon-SiC fluoridated hydroxyapatite-hydroxyapatite multilayered coating on carbon fibers. *Appl. Surf. Sci.* **2019**, *473*, 571–577. [[CrossRef](#)]
34. Batebi, K.; Abbasi Khazaei, B.A.; Afshar, A. Characterization of sol-gel derived silver/ fluor-hydroxyapatite composite coatings on titanium substrate. *Surf. Coat. Technol.* **2018**, *352*, 522–528. [[CrossRef](#)]
35. Yuan, Q.H.; Zhang, Z.Q.; Yang, Y.; Jian, Y.L.; Li, R.L.; Dai, X.Y.; Wu, W.S.; Zhong, J.X.; Chen, C. Synthesis, characterization and biological performance study of Sr-doped hydroxyapatite/chitosan composite coatings. *Mater. Chem. Phys.* **2021**, *270*, 124752. [[CrossRef](#)]
36. Yao, H.-L.; Hu, X.-Z.; Bai, X.-B.; Wang, H.-T.; Chen, Q.-Y.; Ji, G.-C. Comparative study of HA/TiO<sub>2</sub> and HA/ZrO<sub>2</sub> composite coatings deposited by high-velocity suspension flame spray (HVSFS). *Surf. Coat. Technol.* **2018**, *351*, 177–187. [[CrossRef](#)]
37. Mao, Z.-L.; Yang, X.-J.; Zhu, S.-L.; Cui, Z.-D.; Li, Z.-Y. Effect of Na<sup>+</sup> and NaOH concentrations on the surface morphology and dissolution behavior of hydroxyapatite. *Ceram. Int.* **2015**, *41*, 3461–3468. [[CrossRef](#)]